

Controlling the growth of vertically oriented single-walled carbon nanotubes by varying the density of Co—Mo catalyst particles

Liang Zhang, Yongqiang Tan, Daniel E. Resasco *

School of Chemical, Biochemical, and Materials Engineering, University of Oklahoma, 100 E. Boyd, Room T335, Norman, OK 73019, United States

Received 20 December 2005; in final form 16 February 2006

Available online 13 March 2006

Abstract

A simple method to grow vertically aligned arrays of various forms of single-walled carbon nanotubes (V-SWNT) is reported. CO disproportionation on Co—Mo bimetallic catalysts has been used in the synthesis. Resonant Raman and transmission electron microscope (TEM) were employed to characterize the as-produced SWNTs, which display a high purity and very low concentration of other carbon forms. Combination of AFM and SEM gives evidence for the crucial role of the surface distribution of the bimetallic (Co/Mo) catalyst particles on the substrate during the growth of SWNT. A novel growth mechanism is discussed.

© 2006 Elsevier B.V. All rights reserved.

1. Introduction

The in situ growth of aligned CNT on flat substrates has recently become an attractive option for the fabrication of nanotube-based devices such as nanotransistors [1], electron emitters for optoelectronic displays [2], and nanoelectrodes for DNA detection [3]. Alignment of CNT is subcategorized into horizontal alignment (parallel to the surface) and vertical alignment (perpendicular to the surface). Horizontal alignment has been realized by applying electric [4] or magnetic [5] fields or by controlling the direction of the gas flow [6]. Vertical alignment of multi-walled carbon nanotubes has been mastered by researchers for several years [7,8]. However, the growth of vertically aligned SWNT (or V-SWNT) on substrates has remained a challenging task. Only recently, substantial progress has been made on this controlled growth by some research groups in Japan [9–11]. The special environmental conditions required for the V-SWNT growth have been carefully investigated by Maruyama et al. [10,12] who pointed out the importance of achieving total cleanliness in the vacuum chamber where the growth is conducted [10]. Hata and co-

workers [13] have explored the effect of flow rate and the molar ratio of co-feeding gases, ethylene, He, and water. Much less attention has been paid to the state of the catalyst particles, such as the distribution of the metal particles that act as seeds for the growth of the nanotubes. As we describe in the present work, the density and distribution of the catalyst moieties on the flat surface is crucial to determine whether the nanotubes grow in a rather oriented fashion ('forest') or a random network parallel to the surface ('grass'). We have employed SEM and AFM to investigate how the arrangement of bimetallic (Co—Mo) catalyst particles on the substrate affects the resulting morphology of the SWNT. We have found that different forms of SWNT arrays can be reproducibly obtained on flat silicon substrates when the Co—Mo catalyst particles have the appropriate distribution, which can be readily controlled by simply varying the concentration of catalyst solution.

2. Experimental

2.1. Production of SWNT on flat Si substrate

Catalyst solutions of varying metal concentration (0.001–3.8 wt%) were prepared by dissolving salts of Co and Mo into isopropanol, while keeping a constant Co:Mo

* Corresponding author. Fax: +1 405 325 5813.
E-mail address: resasco@ou.edu (D.E. Resasco).

molar ratio of 1:3. Subsequently, a drop of catalyst solution was deposited on a p-type Si wafer. After deposition, the wafer was placed in a covered Petri dish to allow for a slow drying that results in a uniform catalyst film. Following the drying step, the wafer containing the catalyst film was baked in a convection oven at 100 °C for 10 min and then at 500 °C for 15 min.

After pretreatment, the wafer was placed in a quartz reactor, oriented parallel to the direction of the flowing gas. Prior to the production of SWNT by CO disproportionation reaction, the catalyst was heated in H₂ (500 °C), and then in He (750 °C). Subsequently, a 1000 sccm flow of pure CO was initiated at atmospheric pressure. In addition to uniform nanotube growth on uniform catalyst films, patterned nanotube films were prepared by two different methods, one in which the patterns occurred naturally and the other in which we controlled the patterning. Natural patterns were formed when a wet catalyst thin film was dried at a fast drying rate. This method resulted in separate circular droplets of catalysts distributed over the Si substrate. By contrast, the controlled patterning was done by using a mask and sputtering a film of Au–Pd on a previously formed homogeneous catalyst film, prepared by slow drying and calcined in air. In this way, the fraction of catalyst covered by the Au–Pd alloy was selectively deacti-

vated and no nanotube growth occurred on those regions. As a result, the nanotube forest only grew from the remaining active catalyst. The as-produced SWNT were characterized by Raman spectroscopy, electron microscopy (SEM and TEM), and probe microscopy (AFM).

3. Results and discussion

3.1. Influence of catalyst loading on the morphology of SWNT formations

Fig. 1a–c illustrates the dramatic effect of catalyst loading on the resulting morphology of the SWNT formations. This reproducible trend undoubtedly demonstrates that the concentration of the catalyst solution affects the type of SWNT growth on the Si substrate. The SEM images clearly show that vertically aligned (V-SWNT forest) almost 40 μm in length were grown on the substrate impregnated with catalyst solution of 0.19 wt% total metal (Co–Mo) concentration. By contrast, on wafers impregnated with catalyst solutions of 0.38 wt% and 0.02 wt%, random two-dimensional networks of SWNT (grass) were observed after reaction. The sample with higher metal concentration produced a higher nanotube density than the one with

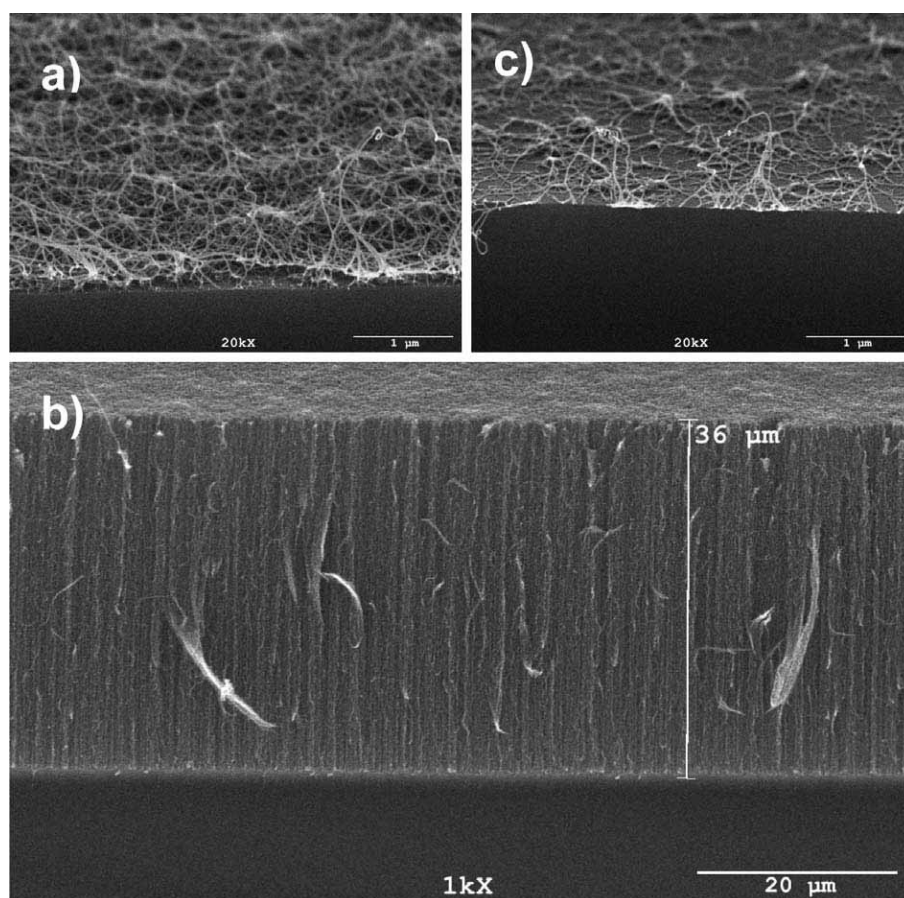


Fig. 1. SEM images of SWNTs produced on silicon wafers with catalyst solution of different concentrations: (a) 0.38%, (b) 0.19%, and (c) 0.02%. Concentration is in total metal weight.

lower metal concentration, but none of them resulted in vertical growth. Apparently, there is an optimum surface concentration of metals that results in vertical growth. Besides, it was observed that grass grown with catalyst solution of higher concentration was reasonably denser than that with catalyst solution of lower concentration. We have explored other concentrations both to higher (up to 3.8 wt%) or lower (0.001 wt%) loadings, but none of them produced V-SWNT forest. In fact, the very high concentration resulted in the formation of carbon fibers and multi-walled carbon nanotubes, while the lowest concentration of catalyst produced mostly scattered thin bundles of SWNT.

The structural characteristics of the nanotubes that make up the forest and grass formations observed by SEM were further evaluated by Raman spectroscopy and TEM. The former is a well-known method for assessing the SWNT quality based on the relative intensity of the D and G bands [14,15]. The latter provides a direct identification of the nature of the carbon species deposited on the surface (i.e., SWNT, MWNT, amorphous, or nanofibers). Raman spectra (as shown in Fig. 2b) of the as-produced V-SWNT forest were obtained with two excitation lasers (633 nm and 488 nm). The very low D/G ratio is consistent with SWNT of high quality with a low concentration of defective nanotubes or disordered carbon species (e.g., nanofibers). At the same time, it is well known that the frequency of the radial breathing mode bands (RBM) is inversely proportional to the nanotube diameter, according to the expression $\omega_{\text{RBM}} = 234/d_{\text{SWNT}} + 10$ (cm^{-1}) [16]. The spectra for the V-SWNT sample obtained with the two different lasers showed that the RBM bands cover a wide frequency range (from 130 cm^{-1} to 300 cm^{-1}), which corresponds to a diameter range 0.8–1.9 nm, a distribution much broader than that typically obtained by the CoMoCAT method on Co–Mo catalysts supported on high-surface area silica [17–19]. The broad distribution of diameters is also reflected in the convergence of the G^- and G^+ features and broad base of the G band [13], in contrast with the sharper lines and more pronounced separation of the G^- and G^+ contributions for the G band in the CoMoCAT material [20]. The TEM observations of the V-SWNT directly taken from the substrate without any purification indicated the presence of nanotubes of varying diameters (Fig. 2a) in agreement with the Raman spectra (Fig. 2b). At the same time, TEM gives ample evidence of the cleanness of the as-prepared V-SWNT; in contrast with samples produced by any other method, they appear free of metal impurities.

To explore the relationship between the metal loading on the substrate and the resulting morphology of the SWNT formations we employed atomic force microscopy (AFM), a powerful tool that provides three-dimensional profiles of surfaces. By investigating the morphology of the catalyst surface before the growth of nanotubes, we were able to identify the optimum distribution of particles that result in V-SWNT forest. This analysis is illustrated in Fig. 3 that contrasts high-magnification SEM pictures of

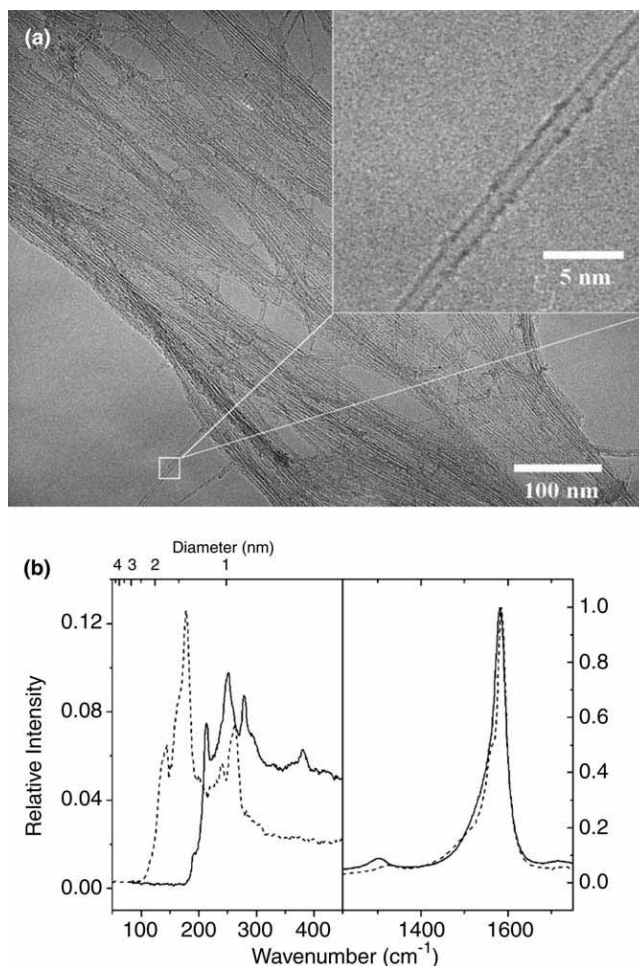


Fig. 2. Structural characterization of VSWNTs: (a) TEM images of VSWNT material removed off the silicon wafer without any purification and (b) Raman spectra of as-produced VSWNTs with excitation lasers of wavelengths 633 nm (solid line) and 488 nm (dashed line).

the SWNT formations and AFM images of calcined catalyst/substrates for three different metal loadings. The AFM image in panel a2 clearly shows that the catalyst particles generated from the impregnating solution with the low metal concentration (0.02 wt%) were small and sparse. From this metal distribution, a similarly sparse formation of two-dimensional SWNT grass was obtained (panel a1). In the case of intermediate metal concentration (0.19 wt%), the AFM in panel b2 evidences a dense population of nano-particles with relatively uniform size. The average distance between these particles was around 60–70 nm. The SEM image (b1) shows that this distribution is successful in promoting the formation of V-SWNT forest. Interestingly, the density of nanotubes bundles is approximately the same as the density of catalyst particles observed by AFM before the growth, which suggest that essentially every catalyst particle is active for the production of nanotubes. By contrast, in the case of 0.38 wt% metal concentration as shown in panel c2, some bigger alloy particles formed on the surface and possibly generated larger cobalt clusters which are not suitable for SWNT

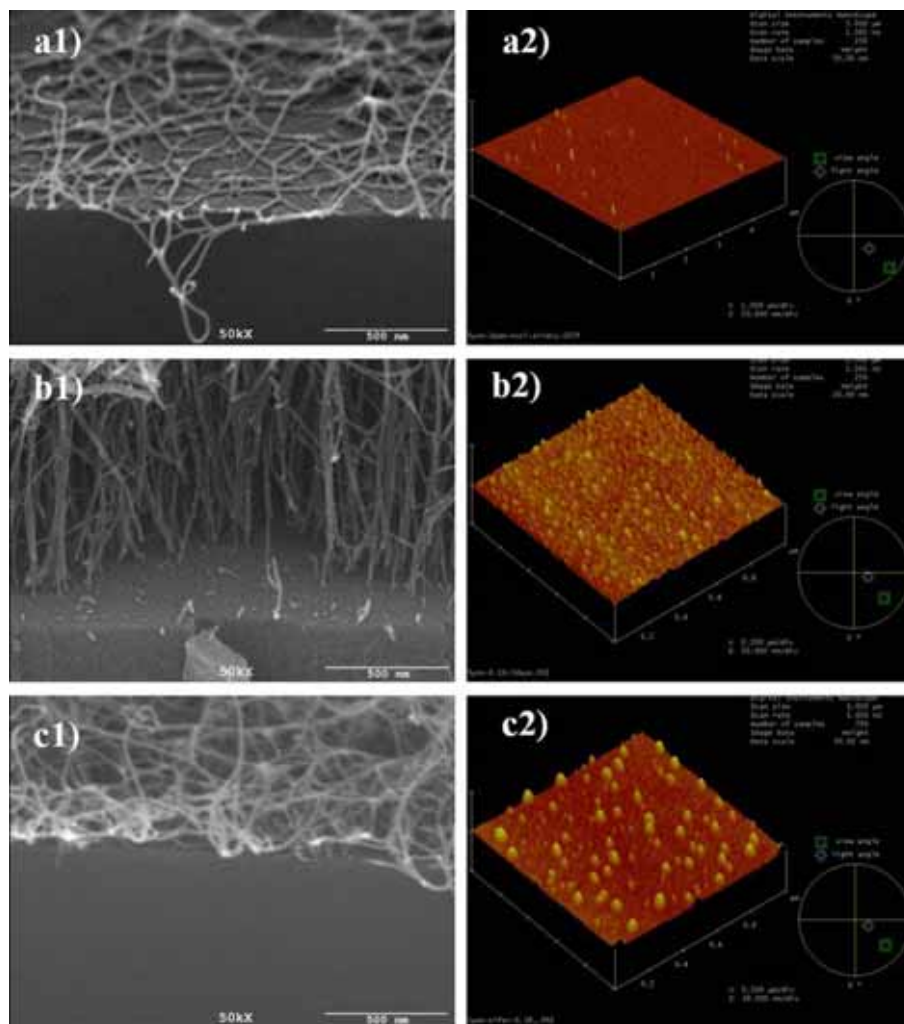


Fig. 3. Side-by-side comparison of SEM pictures (left column) of SWNTs with AFM images (right column) of corresponding silicon wafers with catalyst solution of different concentrations: (a) 0.02 wt% , (b) 0.19 wt%, and (c) 0.38 wt%. Concentration (wt%) refers to total metal weight. AFM images were obtained after the silicon wafers were calcined in oven at 500 °C. All the scale bars in SEM images are 500 nm and the widths of the AFM 3D squares are 1 μ m except the one in panel a2, which is 5 μ m.

nucleation, while a small fraction of Co clusters with the optimum size to grow SWNT still remained between large ones. Thus, a thicker layer of SWNT grass was grown as shown in panel c1.

3.2. Discussion of growth mechanism of vertically oriented SWNT

To explain the strong influence of the catalyst loading on the resulting nanotube morphology we will analyze the growth of nanotubes at three-levels, as illustrated in Fig. 4. The first level of analysis is regarding the growth of each individual SWNT. The TEM observations show that the SWNT grow from the bottom, with the active nano-clusters remaining on the substrate throughout the reaction. As shown in molecular modeling simulations [21,22], following the nucleation step, the nanotube cap forms and is lifted from the cluster surface, leaving metal sites open for a continuous incorporation of carbon atoms

via surface diffusion. The second-order structure to analyze is the formation of bundles of individual tubes, held together by van der Waals forces. Researchers have debated whether an individual catalyst particle produces an individual nanotube, which later bundles up with other nanotubes, or the individual catalyst particle produces a number of nanotubes bundled together from the root. There have been observations that support each of the two possibilities. For example, Gavillet and co-workers [23,24] have reported convincing TEM images that show bundles of SWNT growing from a common catalyst particle. At the same time, Li et al. [25] have reported equally convincing images of individual SWNT produced by individual metal particles, whose size in turn determines the nanotube diameter. We believe that either case is possible to occur depending on the nature of the catalyst and the reaction conditions.

On high surface area supports, which are able to stabilize extremely small metal particles, the one-particle-one-

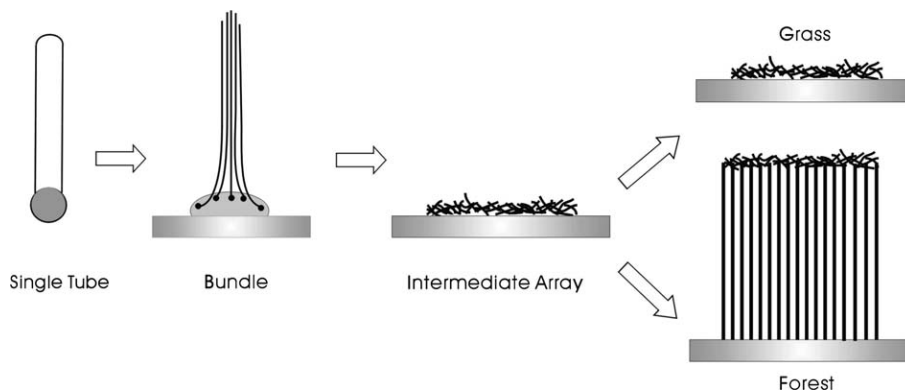


Fig. 4. Schematic diagram illustrating the proposed growth mechanism of third-order structures of VSWNTs: from left to right is first-order structure of a single tube, second-order structure of a bundle, and third-order structure, which can be 2D (xy) grass or 1D (z) forest.

nanotube structure may be prevalent. On bimetallic catalysts, which decompose under reaction conditions generating the active species in-situ, one single bimetallic aggregate can decompose into several nucleation centers, thus giving rise to more than one nanotube per particle. As we have previously proposed for the Co—Mo system,[26] after the treatment in hydrogen the partially reduced cobalt molybdate readily transforms in the presence of CO into molybdenum carbide and cobalt nano-clusters. Experimental results and theoretical calculations [27] have provided evidence to the hypothesis that the main function of molybdenum in Co—Mo catalysts is to act as a matrix that stabilizes the active cobalt nano-clusters. Based on this picture, one can envision the generation of a bundle of several individual SWNT from a single Co—Mo aggregate. The SEM images in Figs. 1 and 3 suggest that individual V-SWNT bundles originate from each of the alloy particles on the substrate.

The third level of analysis addresses the formation of either an ordered array of V-SWNT or a two-dimensional random structure. As shown in this contribution, the average distance between alloy particles plays an important role here. As shown in Fig. 3, the average distance that resulted in the growth of V-SWNT was around 60–70 nm. When the average distance is larger than that, as in the case of 0.02% metal concentration, the SWNT bundles are not able to sustain their upward growth tendency and start bending toward the surface in random direction. In the case of the 0.38% metal concentration, aggregated alloy particles seem to generate large cobalt clusters and due to their non-optimum size lose their ability to template the carbon nucleation for the SWNT growth. Therefore, it is possible that those large clusters become quickly deactivated and as shown in Fig. 3c render part of the surface inactive and make the actual average distance between active particles larger than that necessary for V-SWNT growth.

An important observation needs to be further discussed. When the carbon deposits of a V-SWNT are observed directly perpendicular to the surface, a random network of SWNT bundles is clearly evident over the top of the forest, while the observation at different angles clearly shows

the well-aligned structure shown in Fig. 1b. There is no doubt that, in this case, the root-growth mechanism is operative. Therefore, the nanotube fraction that is observed on top of the forest has been formed during the first stages of reaction, while the ordered growth only occurs later, seemingly constrained by the presence of the two-dimensional crust formed in the initial stages. Initially, a layer of randomly arranged SWNT grows from a loose network to a dense network. The density of this network depends on the surface concentration of the catalyst. With a low concentration of catalyst only a rather loose structure is formed. By contrast, in a region with the proper catalyst density a dense nanotube array forms a crust that constitutes a rather rigid structure. This crust is later lifted up by the growing nanotubes from the bottom (see Fig. 1b). This is the reason why, while each individual nanotube is not perfectly straight and not necessarily every nanotube has the same length, the overall forest has a smooth top surface.

To further demonstrate the effect of the distribution of catalyst particles on the growth of SWNT on flat surfaces, Co—Mo catalysts were patterned over the Si wafer by the two methods described in the experimental section, a natural patterning and a manual patterning. In the case of the natural pattern, fast drying in the air resulted in microscopic circular areas with varying concentration of catalyst. For the manual process, a TEM grid was used as a mask to protect the previously deposited Co—Mo catalyst. The fraction of the surface that was not covered by the grid was deactivated by a film of Au/Pd sputtered over the surface. The resulting patterned growth of V-SWNT obtained by the two methods is illustrated in Fig. 5. Image (a1) shows volcano-shaped SWNT arrays on the substrate patterned by the fast drying method. A cross-sectional image of one of these volcanoes in higher magnification (a2) shows that they comprise vertically aligned SWNT near the edge of the ring, with two-dimensional random arrangements in the middle part. Image (a2) shows parallel V-SWNT bars grown on the active catalyst area defined by the TEM grid. Due to diffusion of Au—Pd from the edge into the space between grid and surface, there is a catalyst

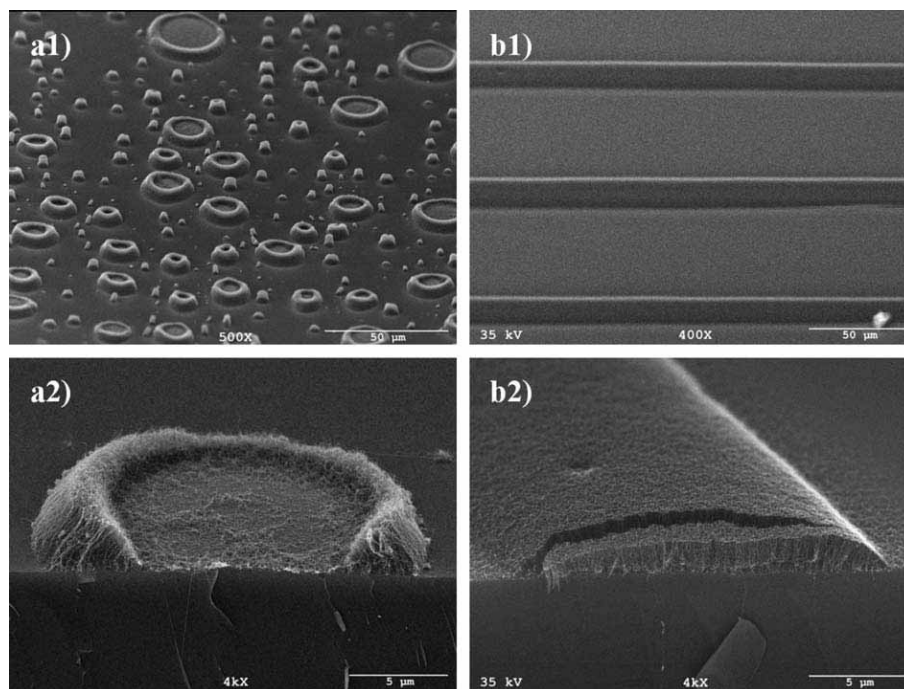


Fig. 5. SEM images of orderly arrays of SWNTs patterned by fast drying process (a) and grid-masked sputter coating (b). Images were taken with lower (1) and higher magnification (2).

concentration gradient in the edge area. As a result, the forest in this area bends towards the outside with the crust on the top extending continuously to the grass attached to the substrate.

Acknowledgements

We gratefully acknowledge the financial support from Department of Energy (Grant DE-FG03-02ER15345) and from the National Science Foundation (Grant No. CTS-0308619). We also thank Bill Chissol and Preston Larson for their help with SEM measurements.

References

- [1] W.B. Choi, J.U. Chu, K.S. Jeong, E.J. Bae, J.W. Lee, J.J. Kim, J.O. Lee, *Appl. Phys. Lett.* 79 (2001) 3696.
- [2] L.M. Dai, *Smart Mater. Struct.* 11 (2002) 645.
- [3] J. Li, H.T. Ng, A. Cassell, W. Fan, H. Chen, Q. Ye, J. Koehne, J. Han, M. Meyyappan, *NanoLetters* 3 (2003) 597.
- [4] Y.G. Zhang, A.L. Chang, J. Cao, Q. Wang, W. Kim, Y.M. Li, N. Morris, E. Yenilmez, J. Kong, H.J. Dai, *Appl. Phys. Lett.* 79 (2001) 3155.
- [5] J.E. Fischer, W. Zhou, J. Vavro, M.C. Llaguno, C. Guthy, R. Haggenueller, M.J. Casavant, D.E. Walters, R.E. Smalley, *J. Appl. Phys.* 93 (2003) 2157.
- [6] S.M. Huang, M. Woodson, R. Smalley, J. Liu, *NanoLetters* 4 (2004) 1025.
- [7] Y.C. Choi, Y.M. Shin, Y.H. Lee, B.S. Lee, G.S. Park, W.B. Choi, N.S. Lee, J.M. Kim, *Appl. Phys. Lett.* 76 (2000) 2367.
- [8] C.J. Lee, D.W. Kim, T.J. Lee, Y.C. Choi, Y.S. Park, Y.H. Lee, W.B. Choi, N.S. Lee, G.S. Park, J.M. Kim, *Chem. Phys. Lett.* 312 (1999) 461.
- [9] G.F. Zhong, T. Iwasaki, K. Honda, Y. Furukawa, I. Ohdomari, H. Kawarada, *Chem. Vapor Depos.* 11 (2005) 127.
- [10] S. Maruyama, E. Einarsson, Y. Murakami, T. Edamura, *Chem. Phys. Lett.* 403 (2005) 320.
- [11] K. Hata, D.N. Futaba, K. Mizuno, T. Namai, M. Yumura, S. Iijima, *Science* 306 (2004) 1362.
- [12] Y. Murakami, E. Einarsson, T. Edamura, S. Maruyama, *Carbon* 43 (2005) 2664.
- [13] D.N. Futaba, K. Hata, T. Yamada, K. Mizuno, M. Yumura, S. Iijima, *Phys. Rev. Lett.* 95 (2005) 056104.
- [14] F. Tuinstra, J.L. Koenig, *J. Chem. Phys.* 53 (1970) 1126.
- [15] M.S. Dresselhaus, P.C. Eklund, *Adv. Phys.* 49 (2000) 705.
- [16] A. Jorio, M.A. Pimenta, A.G. Souza, R. Saito, G. Dresselhaus, M.S. Dresselhaus, *New J. Phys.* 5 (2003) 139.
- [17] S.M. Bachilo, L. Balzano, J.E. Herrera, F. Pompeo, D.E. Resasco, R.B. Weisman, *J. Am. Chem. Soc.* 125 (2003) 11186.
- [18] D.E. Resasco, L. Balzano, J.E. Herrera, O. Matarredona, L. Zhang, *Am. Inst. Phys. Conf. Proc.* 723 (2004) 27.
- [19] F. Hennrich, R. Krupke, S. Lebedkin, K. Arnold, R. Fischer, D.E. Resasco, M.M. Kappes, *J. Phys. Chem. B* 109 (2005) 10567.
- [20] F. Buffa, H. Hu, D.E. Resasco, *Macromolecules* 38 (2005) 8258.
- [21] F. Ding, K. Bolton, A. Rosen, *J. Phys. Chem. B* 108 (2004) 17369.
- [22] F. Ding, A. Rosen, K. Bolton, *Carbon* 43 (2005) 2215.
- [23] J. Gavillet, J. Thibault, O. Stephan, H. Amara, A. Loiseau, C. Bichara, J.P. Gaspard, F. Ducastelle, *J. Nanosci. Nanotech.* 4 (2004) 346.
- [24] J. Gavillet, A. Loiseau, C. Journet, F. Willaime, F. Ducastelle, J.C. Charlier, *Phys. Rev. Lett.* 87 (2001) 275504.
- [25] Y.M. Li, W. Kim, Y.G. Zhang, M. Rolandi, D.W. Wang, H.J. Dai, *J. Phys. Chem. B* 105 (2001) 11424.
- [26] J.E. Herrera, L. Balzano, A. Borgna, W.E. Alvarez, D.E. Resasco, *J. Catal.* 204 (2001) 129.
- [27] (a) J. Zhao, A. Martinez-Limia, P.B. Balbuena, *Nanotechnology* 16 (2005) S575;
(b) P.B. Balbuena, J. Zhao, S. Huang, Y. Wang, N. Sakulchaicharoen, D.E. Resasco, *J. Nanosci. Nanotech.* (in press).